CHARACTERIZATION, MODELING, AND EXPERIMENTAL PETROLOGY OF PICRITIC GREEN GLASS IN NORTHWEST AFRICA 12384: PROBING THE LUNAR MANTLE. C. J.-K. Yen[1], P. K. Carpenter[1], H. Couvy[1], A. J. Irving[2], M. J. Krawczynski[1], and B. L. Jolliff[1], [1]Dept. of Earth and Planetary Sciences and the McDonnell Center for the Space Sciences, Washington University, St. Louis, MO, USA (yenc@wustl.edu), [2]Dept. of Earth & Space Sciences, University of Washington, Seattle, WA, USA.

Introduction: Northwest Africa (NWA) 12384 is a lunar mare basalt breccia [1-3]. A sample such as NWA 12384, with several distinct clasts in one rock, presents an opportunity to test for petrogenetic relationships and whether different breccia components represent different stages of lunar mare volcanism. Lunar volcanic picritic glass beads have been generally assumed to represent near-primary melt compositions of the lunar mantle because they underwent little to no differentiation en route to the surface followed by eruption in volcanic fire-fountains [4-6]. Picritic mare glasses are thus valuable samples for studying the Moon's mantle and volcanic processes. We compared the composition of low-Ti picritic glass beads identified in NWA 12384 with that of other lunar volcanic green glasses in the Apollo sample collection and a few other lunar basaltic meteorites. We then used the NWA 12384 glass bead composition as starting points for crystallization modeling and experiments, to test for petrogenetic relationships between the glass bead and basaltic breccia clasts in NWA 12384.

The fact that none (with one exception) of the previously studied picritic glass compositions is an exact parent via low-pressure fractionation to any of the mare basalt types remains a puzzle [4, 7]. One possibility is that we have a sampling problem of mare volcanic samples. This issue may be improved by meteorite samples which can test global mare compositions [8]. However, a sampling problem may not fully explain the discrepancy between picritic glasses and mare basalts, because crystallization and fractionation processes cannot account for differences in FeO/Sc and light lithophile element concentrations between the two lithologies [9, 10]. This implies that the glasses and basalts may have been derived from different mantle sources.

We identified a large (>0.5 mm across) low-Ti glass bead in NWA 12384 PTS-1 (Fig. 1), and study of the composition (homogeneous, high-Mg) and texture (absence of schlieren and crystallization) confirmed it is a volcanic picritic glass bead. Sixteen compositionally similar volcanic glasses in PTS-1 were identified and analyzed using methods described in [3]. For comparison, data from literature of Apollo green glasses and volcanic glass in other lunar meteorites were compiled [4, 5, 11-16]. Green glasses, specifically, were chosen for comparison because of the low-Ti content of the glass beads in NWA 12384. Titanium is the main compositional discriminator for different lunar volcanic glasses because its concentration spans over an order of magnitude, from <1 to nearly 18 wt.% TiO_2. We modeled crystallization using the composition of the large glass bead under low-pressure low-fO_2 conditions and conducted crystallization experiments under similar conditions. The residual melt compositions in the model and experiments were compared to calculated bulk compositions of basaltic clasts in NWA 12384 (described in [3]) and were found to be similar in major element composition. However, conclusive common liquid lines of descent from the modeling and experimental results that would indicate the NWA 12384 basaltic clast is a direct derivative of the glass bead remain to be seen.

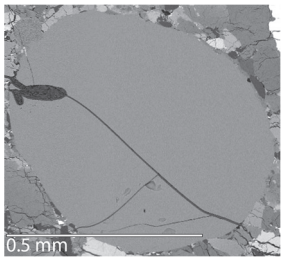

	Large Glass Bead Average (n=14)	Standard Deviation	All Glass Bead Average (n=18)	Standard Deviation
SiO2	44.78	0.24	44.90	0.26
TiO2	0.77	0.02	0.72	0.08
Al2O3	6.67	0.03	6.67	0.05
Cr2O3	0.51	0.02	0.52	0.01
FeO	20.34	0.09	20.68	0.41
MnO	0.27	0.01	0.27	0.02
MgO	18.62	0.07	18.71	0.18
CaO	7.21	0.04	7.31	0.24
Na2O	0.13	0.02	0.09	0.04
K2O	0.03	0.01	0.02	0.01
P2O5	0.04	0.01	0.04	0.02
SO3	0.04	0.01	0.03	0.02
NiO	0.01	0.01	0.01	0.01
Total	99.4	0.3	100.0	0.4
Mg#	62.0	0.15	61.7	0.57

Figure 1. *Backscattered electron image of PTS-1 large volcanic picritic glass bead, and the composition of the large glass bead as well as the average of picritic glasses found.*

Methods: We analyzed the minerals in PTS-1 with a JEOL JXA-8200 electron microprobe at Washington University. This instrument is equipped with 5 wavelength-dispersive spectrometry (WDS) detectors and 1 silicon drift detector for energy-dispersive spectrometry. Spot analyses were made with WDS with an accelerating voltage of 15 kV and a beam current of 25 nA. The spot size was typically 3 μm, but 20 μm and 1 μm spots were used to defocus for a bulk composition and focus for very small features, respectively. Revised modal recombination was done using methods explained in [3] and masking pixels with totals <96% or >103%.

The Apollo green glass data were divided into 5 groups (A~E) defined by [13], which subsequent studies have also followed (Fig. 2). The volcanic glass compositional data were analyzed using the statistical software R, using 95% confidence intervals, unpaired t-tests, and multivariate analysis methods including Q-mode Principal Components Analysis (PCA) and

multidimensional scaling (MDS). PCA has been used previously to identify two arrays among lunar volcanic glasses [17]. MDS was used to transform all eight oxide variables into two for better visualization in 2-D space.

Equilibrium crystallization modeling using MAGPOX was run with the PTS-1 large glass bead average composition as input (Fig. 3) [7, 18]. MAGPOX uses experimental parameterizations of the Ol-Pl-Wo-Qtz model system to predict phases on the liquidus during the evolution (crystallization) of a mafic magma. MAGPOX was chosen over other crystallization models because of better treatment of low fO_2 equilibria. Fractional crystallization modeling using MAGFOX is possible future work. We conducted crystallization experiments with the same composition (excluding Na and K) for powder samples at temperatures between 1125–1250°C, 1 atm pressure, and fO_2 IW-1 using gas mixing Deltech furnaces in the Experimental Geochemistry Lab at Washington University. Experiments were held at temperature over 24–48 hr then rapidly quenched.

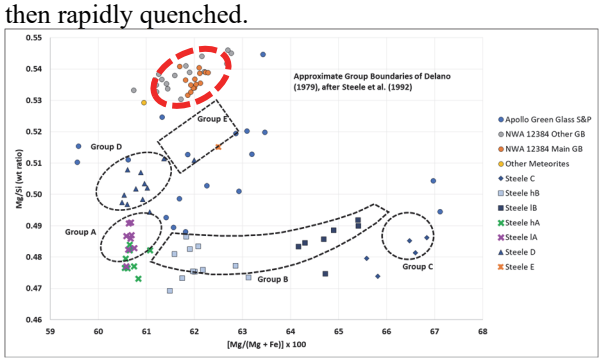

Figure 2. *The Apollo green glasses compared to the volcanic glass in NWA 12384 using the scheme from [13]. Volcanic glasses from the other lunar meteorites except Dhofar 287 plot outside the axis range. S&P refers to [5] and Steele to [15]. Original data defining groups from [13] not included, and analytical uncertainty is small relative to variance.*

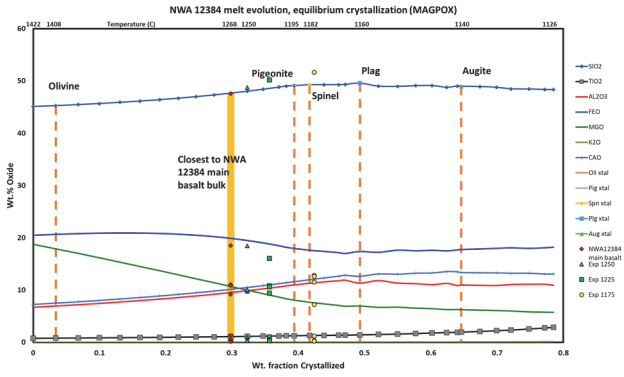

Figure 3 *Melt evolution of MAGPOX equilibrium crystallization model using the NWA 12384 large glass composition as input at 1 bar (low-pressure).*

Results and Discussion: The 95% confidence intervals and unpaired t-tests suggest the volcanic glasses in NWA 12384 do not belong to any of the five previously defined Apollo green glass groups. The Mg and Si visualization also appears to show that the glass beads in NWA 12384 occupy a distinct space outside of the ranges defined by the Apollo green glass groups and is closest in this scheme to Group E (Fig. 2). PCA and MDS plots also show the same behavior, and suggest the compositions follow a trend in PCA and MDS space. Previous studies indicated a distinction between low Mg/Si (A/B/C) and high Mg/Si (D/E), which could represent at least two distinct magma sources [13, 15, 17].

	Clast 3 pigeonite basalt	Model 1268C melt	Model 1250C melt	Exp 1250C melt	Exp 1250C olivine	Clast 3 higher-Fo olivine	Model 1232C melt	Exp 1225C melt	Model 1172C melt	Exp 1175C melt
SiO2	47.56	47.65	48.02	48.76	38.20	37.59	48.40	50.19	49.27	51.65
TiO2	1.28	1.10	1.14	0.97	0.02	0.08	1.18	1.06	1.33	1.23
Al2O3	9.17	9.54	9.88	9.76	0.03	0.38	10.24	10.86	11.58	12.84
Cr2O3	0.40	0.50	0.50	0.49	0.41	0.38	0.50	0.48	0.24	0.37
FeO	18.53	19.88	19.48	18.45	23.54	26.12	19.01	16.07	17.39	12.64
MnO	0.26	0.27	0.26	0.30	0.30	0.27	0.26	0.31	0.24	0.28
MgO	11.05	10.68	9.98	10.00	37.43	33.72	9.30	9.43	7.35	7.22
CaO	10.90	10.14	10.49	10.10	0.33	1.19	10.85	10.63	12.31	11.56
Total	99.2	99.8	99.8	98.8	100.3	99.7	99.8	99.0	99.7	97.79
Mg#	51.5	48.9	47.7	49.1	73.9	69.7	46.6	51.1	43.0	50.5

Table 1. *Summary of selected data from bulk recombination, modeling, and experiment.*

A log-ratio inversion of endmembers MATLAB code (LIME) was used to verify the experimental phase analyses and quantify Fe loss [19]. Fe loss of 0–8 wt.% from high to low temperature was estimated, which is acceptable at these experimental fO_2 conditions. However, this unavoidable Fe loss may explain the discrepancies in FeO, SiO_2, Al_2O_3, and Mg# between the experimental, modeling, and sample compositions (Table 1). The modeling and experimental compositions are in relatively close agreement, excluding FeO. Similarly, the revised bulk recombination for the main basaltic clast in NWA 12384 and the modeled residual melt composition at 1268°C is comparable, with the main differences being in TiO_2 and FeO content. As such, a decisive common liquid line of descent linking the NWA 12384 glass bead and basaltic clasts is not observed. These differences in major element composition would need to be resolved, and after doing so, trace element concentrations need to be measured and modeled to test for discrepancies in light lithophile elements [10].

References: [1] Carpenter, P. et al. (2019a) *LPS L,* Abstract #2148. [2] Carpenter, P. et al. (2019b) *LPS L,* Abstract #2125. [3] Yen, C. et al. (2020) *LPS LI,* Abstract #2804. [4] Delano, J. (1986) *JGR*, *91*, 201–213. [5] Shearer, C. and Papike, J. (1993) *GCA*, *57*, 4785–4812. [6] Elkins-Tanton, L. et al. (2003) *M&PS*, *38*, 515–527. [7] Longhi, J. (1987) *JGR*, *92*, E349–E360. [8] Korotev, R. (2005) *Chem. Erde*, *65*, 297–346. [9] Delano, J. (1990) *LPI Tech Rpt 90-02*, 30-31 [10] Shearer, C. et al. (1994) *GCA*, *58*, 5349–5362. [11] Arai, T. and Warren, P. (1999) *M&PS*, *34*, 209–234. [12] Collareta, A. et al. (2016) *M&PS*, *51*, 351–371. [13] Delano, J. (1979) *LPS X*, 275–300. [14] Demidova, S. et al. (2003) *M&PS*, *38*, 501–514. [15] Steele, A. et al. (1992) *GCA*, *56*, 4075–4090. [16] Zeng, X. et al. (2018) *M&PS*, *53*, 1030–1050. [17] Delano, J. and Livi, K. (1981) *GCA*, *45*, 2137–2149. [18] Longhi, J. (1991) *Amer. Min.*, *76*, 785–800. [19] Krawczynski, M. and Olive, J. (2011) *AGU,* Abstract #V53B–2613.